THE JOURNAL OF PHYSICAL CHEMISTRY Letters

Letter

Cite This: J. Phys. Chem. Lett. 2020, 11, 272−279

pubs.acs.org/JPCL

Nonlocal Subsystem Density Functional Theory

Wenhui Mi[†,‡] and Michele Pavanello*[,†,‡]

[†]Department of Chemistry, Rutgers University, Newark, New Jersey 07102, United States

[‡]Department of Physics, Rutgers University, Newark, New Jersey 07102, United States

Supporting Information

ABSTRACT: By invoking a divide-and-conquer strategy, subsystem DFT dramatically reduces the computational cost of large-scale, *ab initio* electronic structure simulations of molecules and materials. The central ingredient setting subsystem DFT apart from Kohn−Sham DFT is the nonadditive kinetic energy functional (NAKE). Currently employed NAKEs are at most semilocal (i.e., they only depend on the electron density and its gradient), and as a result of this approximation, so far large-scale simulations only included systems composed of weakly interacting subsystems. In this work, we advance the state-of-the-art by introducing fully nonlocal NAKEs in subsystem DFT simulations for the first time. A benchmark analysis based on the S22-5 test set shows that nonlocal NAKEs considerably improve the computed interaction energies and electron densities compared to commonly employed GGA NAKEs, especially when increasing intersubsystem electron density overlap is considered. Most importantly, we resolve the long-standing problem of too attractive interaction energy curves typically resulting from the use of GGA NAKEs.

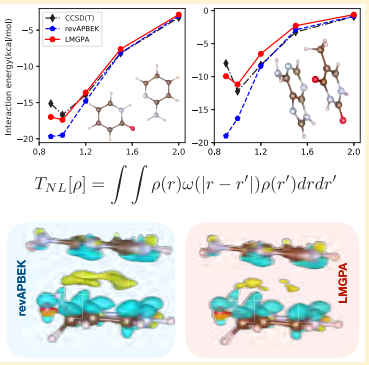

The *ab-initio* model of realistically sized materials has become the ultimate goal for quantum chemistry and material science. To achieve this aim, recent years have witnessed the development of a variety of methods, such as density functional theory (DFT),[1] as well as multilevel/multiscale computational protocols such as QM/MM.[2,3] Quantum embedding methods have recently gained fame, branching into several directions. Among them, subsystem DFT (sDFT) is becoming popular.[4−10] The idea behind sDFT is one of dividing the system into a set of interacting subsystems whose interaction is accounted for approximately in a way that leverages pure density functionals.[11−14] The simplicity of the algorithms involved and the propensity for massive parallelization has driven a number of implementations of sDFT methods in various mainstream quantum simulations codes[15−17] and been successfully applied to a vast array of chemical problems, for instance, structure and dynamics of molecular liquids,[18,19] solvent effects on different types of spectroscopy,[20,21] magnetic properties,[22−26] excited states,[20,27−32] charge transfer states,[33−35] and bulk impurity models.[36]

In sDFT, the total electron density, $\rho(\mathbf{r})$, is expressed as a sum of subsystem contributions. Namely,

$$\rho(\mathbf{r}) = \sum_{I}^{N_S} \rho_I(\mathbf{r}) \tag{1}$$

where N_s is the total number of subsystems considered. The electron density of each subsystem is obtained by variationally minimizing the total energy functional

$$E[\{\rho_I\}] = \sum_{I}^{N_S} E[\rho_I, v_{ext}^I] + \underbrace{T_s[\rho] - \sum_{I}^{N_S} T_s[\rho_I]}_{T_s^{\mathrm{nad}}[\{\rho_I\}]} + \underbrace{E_{xc}[\rho] - \sum_{I}^{N_S} E_{xc}[\rho_I]}_{E_{xc}^{\mathrm{nad}}[\{\rho_I\}]} + \frac{1}{2}\sum_{I\neq J}^{N_s}\int\frac{\rho_I(\mathbf{r})\rho_J(\mathbf{r}')}{|\mathbf{r}-\mathbf{r}'|}d\mathbf{r}d\mathbf{r}' + \sum_{I\neq J}^{N_s}\int\rho_I(\mathbf{r})v_{ext}^J(\mathbf{r})d\mathbf{r} \tag{2}$$

where v_{ext}^J is the external potential associated with subsystem J and by $\{\rho_I\}$ it is intended to indicate the collection of all subsystem densities. The subsystem energy functionals, $E[\rho_I, v_{ext}^I]$, are functionals of both the subsystem external potentials and the subsystem electron densities. The external potential is subsystem-additive (i.e., $v_{ext}(\mathbf{r}) = \sum_I^{N_S} v_{ext}^I(\mathbf{r})$).

Carrying out sDFT simulations involves solving one Kohn−Sham (KS) like equation for each subsystem whose KS potential, $v_{KS}(\mathbf{r})$, is augmented by an embedding potential that accounts for the interactions with all other subsystems. Namely,

$$\left[\frac{-\nabla^2}{2} + v_{KS}^I(\mathbf{r}) + v_{emb}^I(\mathbf{r})\right]\phi_i^I(\mathbf{r}) = \epsilon_i^I(\mathbf{r})\phi_i^I(\mathbf{r}) \tag{3}$$

Received: November 6, 2019
Accepted: December 9, 2019
Published: December 10, 2019

DOI: 10.1021/acs.jpclett.9b03281
J. Phys. Chem. Lett. 2020, 11, 272−279

where $\phi_i^I(\mathbf{r})$ and $v_{emb}^I(\mathbf{r})$ are the KS wave functions and the embedding potential of subsystem I, respectively. The embedding potential can be written as follows:[6,7]

$$v_{emb}^I(\mathbf{r}) = \sum_{J\neq I}^{N_s}\left[\int \frac{\rho_J(\mathbf{r}')}{|\mathbf{r}-\mathbf{r}'|}d\mathbf{r}' + \sum_J v_{ext}^J(\mathbf{r})\right] + \frac{\delta T_s^{nad}[\{\rho_I\}]}{\delta\rho_I(\mathbf{r})} + \frac{\delta E_{xc}^{nad}[\{\rho_I\}]}{\delta\rho_I(\mathbf{r})} \quad (4)$$

In the above, T_s and E_{xc} are kinetic energy density functionals (KEDF) and exchange-correlation (xc), respectively.

In KS-DFT, $T_s[\rho]$ is evaluated exactly from the KS orbitals of the system. Conversely, in a sDFT scheme, approximate nonadditive kinetic energy functionals (NAKE, defined in eq 2) are used. Employing NAKE constitutes the most important and crucial difference between KS-DFT and sDFT.[37,38]

NAKEs are typically derived from semilocal KEDFs[37] and have been at most of Laplacian level.[39] However, it is common knowledge that semilocal NAKEs cannot approach a regime in which the subsystem electron densities strongly overlap where they typically give wrong interaction energy curves.[40,41] These limitations originate from the natural nonlocality of the underlying KEDF[42] and in turn of the NAKEs. In this work, we tackle these issues by employing state-of-the-art nonlocal KEDFs to generate NAKEs.

There are interesting new developments regarding nondecomposable NAKE approximants[43] which are reported to be able to describe covalent bonds in the molecules Na_2, Li_2. Even though we do not consider them here, we will evaluate their performance in a follow up publication.

Even though nonlocal KEDFs have a long history in OF-DFT simulations,[44−46] to the best of our knowledge they have not yet been employed as NAKEs. This is probably because in sDFT, the distribution of electron densities is usually more localized compared to the electron density of the supersystem.[47−49] Thus, when developing nonlocal NAKEs, KEDFs must be able to correctly simulate both homogeneous and nonhomogeneous systems and be numerically stable.

The ability to approach inhomogeneous systems is the most challenging property to satisfy because the nonlocal KEDFs have been historically developed for extended metallic systems whose electron density is close to uniform. The typical ansatz chosen for nonlocal functionals is

$$T_s[\rho] = \underbrace{T_{TF}[\rho] + T_{vW}[\rho]}_{T_{TV}[\rho]} + T_{NL}[\rho] \quad (5)$$

where $T_{TF}[\rho]$ is the Thomas−Fermi (TF) functional,[50,51] $T_{vW}[\rho]$ is the von Weizsäcker (vW) functional,[52] and $T_{NL}[\rho]$ is the nonlocal part. The corresponding KEDF potential can be written as

$$v_{T_s}(\mathbf{r}) = \frac{\delta T_{TV}[\rho]}{\delta\rho(\mathbf{r})} + \frac{\delta T_{NL}[\rho]}{\delta\rho(\mathbf{r})} = v_{TV}(\mathbf{r}) + v_{NL}(\mathbf{r}) \quad (6)$$

where $v_{TV}(\mathbf{r})$ is the Thomas−Fermi−vW potential which we will later discuss. The nonlocal part is defined by a double integration of the electron density evaluated at two different points in space and an effective interaction, the so-called kernel, ω:

$$T_{NL}[\rho] = \int\int \rho^\alpha(\mathbf{r})\omega[\rho](\mathbf{r},\mathbf{r}')\rho^\beta(\mathbf{r}')d\mathbf{r}d\mathbf{r}' \quad (7)$$

where α and β are positive numbers. The kernel is related to the second functional derivative of the KEDF with respect to the electron density[53] and is typically approximated by a function of only $|\mathbf{r}-\mathbf{r}'|$.

The available nonlocal KEDFs,[54−61] can be categorized in functionals whose kernel only depends on the average electron density (i.e., ρ_0 which is well-defined only for condensed-phase systems) and functionals whose kernel instead depends on the total electron density and not just its average.[57] Clearly, nonlocal KEDFs with a density-independent kernel cannot be directly employed as NAKEs because the presence of the restrictive parameter, ρ_0, would make the KEDF unable to approach inhomogeneous systems. Unfortunately, some KEDFs with density dependent kernels are either too expensive (i.e., HC[56] which we expect to also behave well when employed as NAKE) or numerically unstable for arbitrary inhomogeneous systems (i.e., WGC[55]); thus, we will not employ them here.

We recently proposed a new series of nonlocal KEDFs featuring local density dependent kernels which we showed[62] can predict accurately the electron density, energy, and forces for clusters of metallic and group III and V atoms. These functionals are based on and generalize existing functionals with density independent kernels (such as WT,[57] MGPA, and MGPG functionals[58]). The generalization allows them to approach inhomogeneous systems because they feature fully density dependent kernels.[62]

In our previous study of the LMGP family of KEDFs,[62] we also analyzed the corresponding potentials and compared them against the exact KS-DFT for isolated pseudoatoms (i.e., atoms described by a pseudopotential). We noted that LMGP improves upon the GGA local and semilocal potential, and particularly it delivers potentials which are less repulsive in the high-density regions. This results in a more localized electron density, closer to the result obtained with the exact KEDF functional (i.e., KS-DFT). In this work, we leverage on this improved behavior of the LMGP family of KEDF, which will translate into higher quality NAKEs.

Let us summarize the employed kernels, starting with the WT kernel[57] expressed in reciprocal space (q is the reciprocal space variable for $|\mathbf{r}-\mathbf{r}'|$) and $\eta(q) = \frac{q}{2k_F}$ with k_F being the Fermi wavevector),

$$\omega_{WT}(q) = \frac{6}{5}\frac{\pi^2}{(3\pi^2)^{1/3}}G_{NL}(\eta(q)) \quad (8)$$

which then is modified to satisfy functional integration relations[58] by the addition of one correction term. Namely,

$$\omega_{x,y}(q) = \omega_{WT}(q) - \frac{\pi^2 x}{(3\pi^2)^{1/3}}\int_0^1 dt\, t^y \frac{dG_{NL}(\eta(q,t))}{dt} \quad (9)$$

where

$$G_{NL}(\eta) = \left(\frac{1}{2} + \frac{1-\eta^2}{4\eta}\ln\left|\frac{1+\eta}{1-\eta}\right|\right)^{-1} - 3\eta^2 - 1 \quad (10)$$

and MGP is given by $(x,y) = \left(\frac{6}{5},\frac{6}{5}\right)$, MGPA by $(x,y) = \left(\frac{3}{5},\frac{6}{5}\right)$, and MGPG by $(x,y) = \left(\frac{6}{5},\frac{3}{5}\right)$. The only

DOI: 10.1021/acs.jpclett.9b03281
J. Phys. Chem. Lett. 2020, 11, 272−279

difference between MGP/A/G is the way a kernel is symmetrized. We refer the interested reader to the Supporting Information of ref 58.

In ref 62 we developed a technique to generalize WT, MGP/A/G functionals to approach localized, finite systems by invoking spline techniques to obtain kernels no longer dependent only on the average electron density but instead they are dependent (locally) on the full electron density function. In this way, we generate the LWT, LMGP/A/G functionals from the kernels mentioned in eqs 8−9.

At implementation time, we noticed that the terms $T_{TV} = T_{TF} + T_{vW}$ and T_{NL} each can lead to numerical instability for different reasons. The issue for $T_{TV}[\rho]$ originates from its quadratic dependence on the density gradient. In the typical GGA formalism:

$$T_{TV}[\rho] = \int t_{TF}(\mathbf{r}) F_{TV}(s(\mathbf{r}))d\mathbf{r} \tag{11}$$

where s is the dimensionless reduced density gradient, $s = \frac{|\nabla\rho|}{2\rho k_f} = \frac{1}{2(3\pi^2)^{1/3}}\frac{|\nabla\rho|}{\rho^{3/4}}$, the enhancement factor $F_{TV}(S) = 1 + \frac{5}{3}s^2$, and $t_{TF}(\mathbf{r}) = \frac{3}{10}(3\pi^2)^{2/3}\rho^{5/3}(\mathbf{r})$. Numerical inaccuracies arise at large s because in this limit, $F_{TV}(s)$ is unbound and the error in the density becomes uncontrollable.

Thus, we need to find a proper way to cap $F_{TV}(s)$ for large s. To achieve this aim, we borrow a formalism similar to PBE exchange[63] and reshape the enhancement factor of Thomas−Fermi (TF) plus von Weizsäcker (vW) kinetic energy functional in a stable formalism (named STV):

$$F_{STV}(s) = 1.0 + \frac{5}{3}\frac{s^2}{1.0 + as^2} \tag{12}$$

In this formalism, when $a = 0$, $F_{STV}(s)$ is the same as the original F_{TV}; by increasing a, F_{STV} smoothly approaches a constant number for large s, which should ameliorate the numerical inaccuracies. Figure 1 compares STV functionals (for both $a = 0.1$ and 0.01) with the T_{TV} and revAPBEK enhancement factors.

In addition to the numerical problem for the T_{TV} KEDF, the nonlocal KEDF potentials also need to be carefully implemented in the low electron density regions. The nonlocal kinetic potentials for all the nonlocal functionals considered in this work share the form:

$$v_{NL}(\mathbf{r}) = \rho^{-1/6}(\mathbf{r})F^{-1}[\tilde{\rho}^{5/6}(\mathbf{q})\omega(q)](\mathbf{r}) \tag{13}$$

where $\tilde{\rho}^{5/6}(\mathbf{q}) = F[\rho^{5/6}(\mathbf{r})](\mathbf{q})$, $\omega(q)$ is the nonlocal kernel expressed in reciprocal space, F and F^{-1} represent the fast Fourier transform and inverse fast Fourier transform, respectively. In eq 13 it is made clear that we approximate the real-space kernel as a function of only $|\mathbf{r} - \mathbf{r}'|$ resulting in a dependence on only the magnitude of the reciprocal space vector $q = |\mathbf{q}|$. In the same equation there is a $\rho^{-1/6}(\mathbf{r})$ prefactor, which is numerically noisy in the low electron density regions. To eliminate this issue, a local density weighted mix of GGA and nonlocal kinetic potential scheme is proposed:

$$v_{T_s}[\rho](\mathbf{r}) = (v_{NL}[\rho](\mathbf{r}) + v_{STV}[\rho](\mathbf{r}))W[\rho](\mathbf{r}) + v_{GGA}[\rho](\mathbf{r})(1 - W[\rho](\mathbf{r})) \tag{14}$$

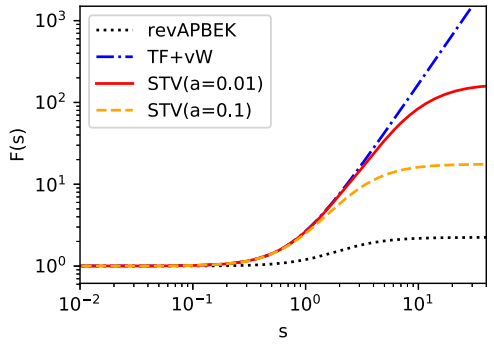

Figure 1. Enhancement factors associated with the following functionals: T_{STV} (smooth version of the T_{TV}) with $a = 0.01$ in red solid line, $a = 0.1$ in orange dashed line, original T_{TV} in blue dot−dash line, and revAPBEK in black dotted line.

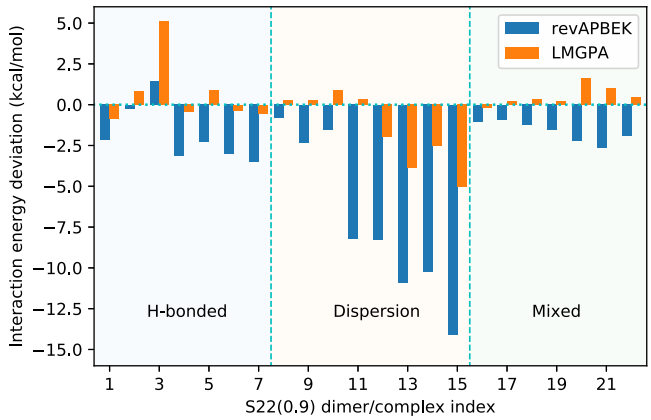

Figure 2. Interaction energy deviations in kcal/mol between sDFT with revAPBEK and LMGPA NAKE functionals against the corresponding KS-DFT results. PBE xc functional is adopted in both sDFT and KS-DFT calculations. All geometries are taken from the S22(0.9) set. The indices in the x-axis correspond to complexes listed in Table S1 of the Supporting Information.

Table 1. Summary of the Root-Mean-Square Deviations (RMSD) of the Interaction Energies Computed with sDFT Carried out with revAPBEK and LMGPA NAKEs and the PBE xc Functional against KS-DFT Results[a]

NAKEs	Hydrogen	Dispersion	Mixed	Total
revAPBEK	2.49	8.42	1.76	5.36
LMGPA	2.05	2.54	0.77	1.97

[a]All geometries are from the S22(0.9) set, and RMSDs are in kcal/mol.

where $W[\rho](\mathbf{r}) = \frac{\rho(\mathbf{r})}{\rho_{max}}$, ρ_{max} is the maximum value of electron density in the system, and v_{GGA} is the KEDF potential from a GGA functional (here we choose revAPBEK). In this way, for the region of space with low electron density, the kinetic potential is mainly contributed by the GGA functional instead of the nonlocal part. The procedure in eq 14 cures the numerical instability of the nonlocal part of the potential.

With the KEDF potential in hand, the kinetic energy can be evaluated by line integration:

$$T_s[\rho] = \int \rho(\mathbf{r})d\mathbf{r} \int_0^1 v_{T_s}[\rho_t](\mathbf{r})dt \tag{15}$$

where $\rho_t(\mathbf{r}) = t\rho(\mathbf{r})$.

DOI: 10.1021/acs.jpclett.9b03281
J. Phys. Chem. Lett. 2020, 11, 272−279

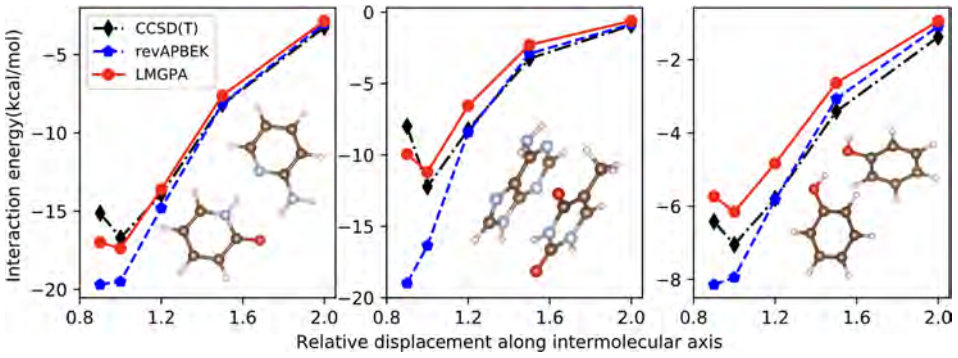

Figure 3. Interaction energies obtained by sDFT with revAPBEK and LMGPA NAKEs in conjunction with rVV10 xc functional compared against CCSD(T).

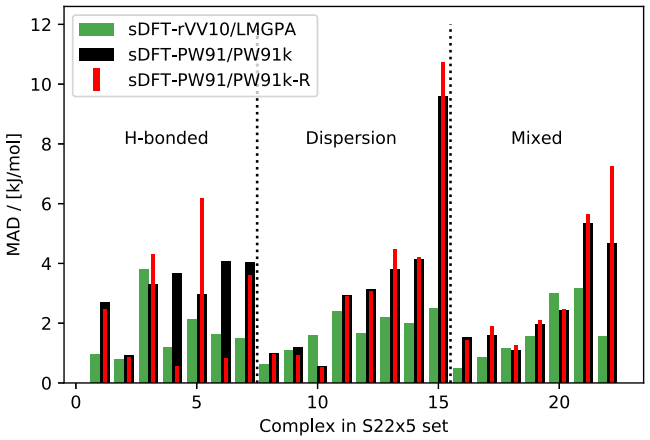

Figure 4. Mean absolute deviations (MADs) of interaction energies per molecule for the nonlocal sDFT-rVV10/LMGPA in comparison to semilocal sDFT-PW91/PW91k and sDFT-PW91/PW91k-R results for the S22x5 test set. The semilocal sDFT results are taken from ref 41. All values are given in kJ/mol/molecule.

Table 2. RMSD of the $\langle\Delta\rho\rangle$ Values (Defined in Eq 16) Obtained by sDFT with Different NAKEs (revAPBEK and LMGPA) for the S22-5 Test Set

r/r_0	0.9	1.0	1.2	1.5	2.0
revAPBEK	0.0600	0.0370	0.0148	0.0042	0.0008
LMGPA	0.0583	0.0361	0.0148	0.0042	0.0008

Table 3. RMSD of $\langle\Delta\rho\rangle$ Values (Defined in Eq 16) Arranged by Bonding Type in the S22(0.9) Set

Bond type	Hydrogen	Dispersion	Mixed	Total
revAPBEK	0.0805	0.0600	0.0270	0.0600
LMGPA	0.0801	0.0561	0.0261	0.0583

We now present pilot calculations aimed at assessing the performance of our newly proposed nonlocal NAKEs based on the following KEDFs: LWT, LMGPA, and LMGPG. We select the S22-5 test set (noncovalently interacting complexes at equilibrium and displaced geometries[64]) as benchmarks. The molecules are placed in an orthorhombic (cubic) box where the periodic boundary condition is applied. The separations between the studied molecules and their nearest-neighbor periodic images are at least 12 Å. This is a large enough separation to ensure that spurious self-interactions are negligible. Both our new proposed nonlocal NAKEs and the GGA functionals have been implemented in a development version of the embedded Quantum ESPRESSO (eQE) package.[16] All KS-DFT benchmark calculations are performed with the Quantum ESPRESSO (QE) package.[65] In both subsystem DFT and KS-DFT calculations, the Perdew–Burke–Ernzerhof (PBE) form of the GGA xc functional[63] is employed. In order to show the influence of the xc functional on the results, the nonlocal rVV10[66] functional is also adopted. Ultrasoft pseudopotentials are adopted[67] (specifically the GBRV version 1.4[68]). The plane wave cutoffs are 70 and 400 Ry, for the wave functions and density, respectively.

When comparing the interaction energies summarized in Figure S1 of the Supporting Information,[69] both the revAPBEK and LMGPA functional reproduce the benchmark within 2 kcal/mol for weakly interacting systems. Decreasing the separation between two fragments from S22(2.0) to S22(0.9) (S22(x) indicates that the distance between the two fragments is given by $x \times R_{eq}$, where R_{eq} is the equilibrium distance as computed by coupled cluster theory), as by expectations increases the deviation of sDFT and KS-DFT interaction energies. To clearly show the performance of LMGPA and the revAPBEK functionals for strongly interacting configurations, here we focus on the interaction energies and total electron densities (i.e., the sum of the two subsystems' densities for sDFT and the total density for KS-DFT) computed for the S22(0.9) case. Results for all other systems are provided in the Supporting Information.[69] Figure 2 shows that the LMGPA functional considerably improves the revAPBEK results for all systems with a maximum deviation of the interaction energy of about 5 kcal/mol. This compares quite well against more than 14 kcal/mol for revAPBEK. The only exception is the formic acid dimer in which the two fragments are bonded by a double hydrogen bond. The abnormality of this dimer is revealed in two aspects: it is the only case where the revAPBEK functional overestimates the total energy, and it also is the only case where the revAPBEK functional performs better than LMGPA. This system is also associated with the largest electron density deviation (*vide infra*), and thus the revAPBEK apparent good performance is due to fortuitous error cancellation.

To further quantify the performance of the LMGPA NAKE functional, we summarize the root-mean-square deviations (RMSD) of the interaction energies sDFT with different NAKEs (revAPBEK and LMGPA) from the reference KS-DFT results shown in Table 1. Inspecting the table, it is clear that LMGPA outperforms revAPBEK. The total RMSD for LMGPA is just 1.97 kcal/mol, while revAPBEK results in a RSMD of 5.36 kcal/mol, which is about three times larger than

DOI: 10.1021/acs.jpclett.9b03281
J. Phys. Chem. Lett. 2020, 11, 272−279

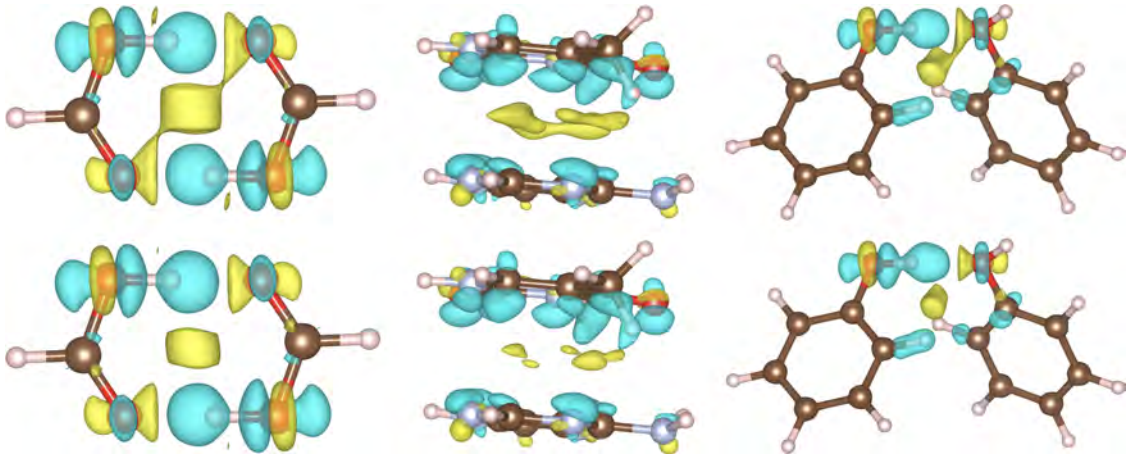

Figure 5. $\langle \Delta\rho \rangle$ (defined in eq 16) calculated with two NAKEs: revAPBEK (top) and LMGPA (bottom). PBE xc functional is adopted in both sDFT and KS-DFT calculations. Isosurface cutoffs are as follows (L-to-R): 10^{-3}, 5.0×10^{-4}, 5.0×10^{-4}.

the LMGPA RMSD. We notice that the LMGPA particularly improves the dispersion bound systems for which it obtains much improved results (2.54 kcal/mol) compared to revAPBEK (8.42 kcal/mol). Moreover, the long-standing issue of GGA NAKEs that generate too attractive interaction energy curves (which is also clear from Figure 2) is cured by the LMGPA NAKE functional.

It is now clear that LMGPA delivers good interaction energies with deviations from KS-DFT below 5 kcal/mol (average deviation of less than 2 kcal/mol). We wish to test its ability to deliver accurate interaction energies in comparison to the benchmark CCSD(T) energies.[64,70] In a previous formal work by our group[40] we showed that once sDFT is associated with an exact T_s^{nad} and a nonlocal xc functional, interaction energies become closer to benchmark results. Thus, here we compare LMGPA and revAPBEK NAKEs in conjunction with the rVV10 xc functional. Due to its nonlocal nature, rVV10 has been shown to be much more reliable than GGA xc functionals in KS-DFT calculations,[71] especially for the dispersion bonded systems. In this work, we witness a similar outcome as evident from the benchmarks for each type of bonding systems showed in Figure 3. KS-DFT with both PBE and rVV10 xc functionals are available in the Supporting Information.[69] As shown in Figures S4−5, KS-DFT with rVV10 functional can obtain nearly exactly the same results as CCSD(T) for all systems. Figure 3 indicates that in line with the results presented above, LMGPA obtains correct equilibrium bonding length and the order of energies. This is a major improvement in comparison to the revAPBEK results which feature a well characterized deficiency of too attractive energy curves.[18,40,41] Moreover, in order to show the influence of the choice of xc functionals on the sDFT performance, we benchmarked the sDFT interaction energy deviations from the corresponding KS-DFT results. As shown in Figure S6, the sDFT results are nearly independent from the choice of xc functional, further reinforcing the conclusion that the nonlocal LMGPA functional resolved the long-standing problem of too attractive energy curves computed by semilocal NAKEs.

It is known that sDFT relies on error cancellation for the description of weak intermolecular interactions. For example, sDFT reproduces the structure and dynamics of molecular liquids[18,19] and can reproduce some (not all) interaction energy curves such as the ones presented in Figure S9. Thus, it is not surprising that when a better NAKE is employed, the agreement against the CCSD(T) benchmark does not necessarily improve. In Figure 4, we reproduce Figure 14 of ref 41, including our nonlocal sDFT results. It is clear from the figure that when accurate NAKE and xc functionals are used, the agreement against the benchmark improves substantially.

We list in Table S3 the numerical values of the interaction energies for the S22 set computed with PBE/revAPBEK and rVV10/LMGPA against the CCSD(T) reference. There we see that the new nonlocal sDFT does not deteriorate the documented good performance of semilocal sDFT for this data set.[40,41]

Reproducing the electron density is also important in evaluation of the performance of functionals.[72,73] Thus, a more insightful comparison is made by calculating the number of electrons misplaced by sDFT, $\langle \Delta\rho \rangle$, defined as

$$\langle \Delta\rho \rangle = \frac{1}{2} \int |\rho_{sDFT}(\mathbf{r}) - \rho_{KS}(\mathbf{r})| d\mathbf{r} \tag{16}$$

This value is an important quantity, as it vanishes only when sDFT and KS-DFT electron densities coincide. The RMSD of $\langle \Delta\rho \rangle$ for revAPBEK and LMGPA NAKEs results are showed in Table 2. As expected, when the interaction between the two subsystems transitions from weak to strong (corresponding to from S22(2.0) to S22(0.9)), the $\langle \Delta\rho \rangle$ value also increases. For the S22(0.9) and S22(1.0) sets, LMGPA performs slightly better than revAPBEK. Since in the weak interaction regime for both NAKEs can generate nearly the same and accurate electron density, we will just focus on the set with the strongest interactions (i.e., the S22(0.9)).

The results for each bonding type are summarized in Table 3. Compared with revAPBEK, LMGPA NAKE obtains smaller $\langle \Delta\rho \rangle$ for all cases indicating that it can generate more accurate electron density for all types of bonding. We select the complexes which generate the largest $\langle \Delta\rho \rangle$ for each type of bonding and plot the corresponding isosurface plots of density difference (compared with KS-DFT) for sDFT with revAPBEK and LMGPA; see Figure 5. As expected, the density difference mainly occurs on the overlap regions between the two subsystems. We now have a visual of the fact that LMGPA can generate more accurate electron densities compared to revAPBEK, since the density difference region is much smaller than the revAPBEK results.

In the previous analysis, we focused on LMGPA with a = 0.01 in the definition of the smooth Thomas−Fermi−von

DOI: 10.1021/acs.jpclett.9b03281
J. Phys. Chem. Lett. 2020, 11, 272−279

Weizsäcker, STV, functional eq 12. To benchmark the influence of the choice of a and the performance of each kernel, both a = 0.01 together with a = 0.1 and other functionals (LWT and LMGPG) are also compared in the Supporting Information.[69] As shown in Figure S2, all these nonlocal functionals result in improved interaction energies compared against revAPBEK. In terms of electron density, Figures S7 and S8 show that all of the new nonlocal NAKEs obtain better results than revAPBEK.

In conclusion, for the first time we employed nonlocal nonadditive kinetic energy functionals in subsystem DFT simulations. Our approach relies on (1) adopting latest-generation nonlocal functionals featuring a fully density dependent kernel, correctly tackling systems with localized and inhomogeneous electron density; (2) suppressing numerical instabilities in the evaluation of the von Weizsäcker KEDF and nonlocal KEDF in the low electron density regions. Our approach leads to numerically stable and accurate subsystem DFT simulations. Benchmark tests against the well-known S22-5 test set indicate that our new approach not only can reproduce accurate interaction energies across bonding types (hydrogen, dispersion, and mixed), but we also better reproduce the benchmark electron density. In addition, the new nonlocal subsystem DFT approach (that includes nonlocal NAKE and nonlocal xc functional) obtains correct equilibrium bonding lengths and correct shape of the energy curves compared to CCSD(T) energy curves, which have been a long-standing challenge for semilocal sDFT.

■ ASSOCIATED CONTENT

Supporting Information

The Supporting Information is available free of charge at https://pubs.acs.org/doi/10.1021/acs.jpclett.9b03281.

Interaction energy deviations; S22-5 dimer/complex and corrresponding index number; total energy deviations; $\langle\Delta\rho\rangle$; $\langle\Delta\rho\rangle_{\mathrm{NAKE}}/\langle\Delta\rho\rangle_{\mathrm{revAPBEK}}$ ratio; and potential energy curves (PDF)

■ AUTHOR INFORMATION

Corresponding Author

*E-mail: m.pavanello@rutgers.edu.

ORCID

Michele Pavanello: 0000-0001-8294-7481

Notes

The authors declare no competing financial interest.

■ ACKNOWLEDGMENTS

We gratefully acknowledge discussions with Pablo Ramos and Xuecheng Shao. This material is based upon work supported by the National Science Foundation under Grant No. CHE-1553993. The authors acknowledge the Office of Advanced Research Computing (OARC) at Rutgers, The State University of New Jersey for providing access to the Amarel cluster and associated research computing resources that have contributed to the results reported here. URL: http://oarc.rutgers.edu.

■ REFERENCES

(1) Kohn, W.; Sham, L. J. Self-Consistent Equations Including Exchange and Correlation Effects. *Phys. Rev.* **1965**, *140*, 1133−1138.

(2) Senn, H. M.; Thiel, W. QM/MM Methods for Biomolecular Systems. *Angew. Chem., Int. Ed.* **2009**, *48*, 1198−1229.

(3) Shurki, A.; Warshel, A. Structure/Function Correlations of Proteins Using MM, QM/MM, and Related Approaches: Methods, Concepts, Pitfalls, and Current Progress. *Adv. Protein Chem.* **2003**, *66*, 249−313.

(4) Wesolowski, T. A.; Shedge, S.; Zhou, X. Frozen-Density Embedding Strategy for Multilevel Simulations of Electronic Structure. *Chem. Rev.* **2015**, *115*, 5891−5928.

(5) Gomes, A. S. P.; Jacob, C. R. Quantum-chemical embedding methods for treating local electronic excitations in complex chemical systems. *Annu. Rep. Prog. Chem., Sect. C: Phys. Chem.* **2012**, *108*, 222−277.

(6) Jacob, C. R.; Neugebauer, J. Subsystem density-functional theory. *WIREs: Comput. Mol. Sci.* **2014**, *4*, 325−362.

(7) Krishtal, A.; Sinha, D.; Genova, A.; Pavanello, M. Subsystem Density-Functional Theory as an Effective Tool for Modeling Ground and Excited States, their Dynamics, and Many-Body Interactions. *J. Phys.: Condens. Matter* **2015**, *27*, 183202.

(8) Nafziger, J.; Wasserman, A. Density-Based Partitioning Methods for Ground-State Molecular Calculations. *J. Phys. Chem. A* **2014**, *118*, 7623−7639.

(9) Senatore, G.; Subbaswamy, K. Density dependence of the dielectric constant of rare-gas crystals. *Phys. Rev. B: Condens. Matter Mater. Phys.* **1986**, *34*, 5754.

(10) Wesolowski, T. A.; Warshel, A. Frozen Density Functional Approach for *ab Initio* Calculations of Solvated Molecules. *J. Phys. Chem.* **1993**, *97*, 8050.

(11) Yang, W. Direct Calculation of Electron Density in Density-Functional Theory. *Phys. Rev. Lett.* **1991**, *66*, 1438−1441.

(12) Huang, C.; Pavone, M.; Carter, E. A. Quantum mechanical embedding theory based on a unique embedding potential. *J. Chem. Phys.* **2011**, *134*, 154110.

(13) Gritsenko, O. V. In *Recent Advances in Orbital-Free Density Functional Theory*; Wesolowski, T. A., Wang, Y. A., Eds.; World Scientific: Singapore, 2013; Chapter 12, pp 355−365.

(14) Goodpaster, J. D.; Ananth, N.; Manby, F. R.; Miller, T. F., III Exact Nonadditive Kinetic Potentials for Embedded Density Functional Theory. *J. Chem. Phys.* **2010**, *133*, 084103.

(15) Jacob, C. R.; Neugebauer, J.; Visscher, L. A Flexible Implementation of Frozen-Density Embedding for Use in Multilevel Simulations. *J. Comput. Chem.* **2008**, *29*, 1011−1018.

(16) Genova, A.; Ceresoli, D.; Krishtal, A.; Andreussi, O.; DiStasio, R., Jr.; Pavanello, M. eQE — A Densitiy Functional Embedding Theory Code For The Condensed Phase. *Int. J. Quantum Chem.* **2017**, *117*, No. e25401.

(17) Andermatt, S.; Cha, J.; Schiffmann, F.; VandeVondele, J. Combining Linear-Scaling DFT with Subsystem DFT in Born−Oppenheimer and Ehrenfest Molecular Dynamics Simulations: From Molecules to a Virus in Solution. *J. Chem. Theory Comput.* **2016**, *12*, 3214−3227.

(18) Mi, W.; Ramos, P.; Maranhao, J.; Pavanello, M. Ab Initio Structure and Dynamics of CO2 at Supercritical Conditions. *J. Phys. Chem. Lett.* **2019**, *10*, 7554−7559.

(19) Genova, A.; Ceresoli, D.; Pavanello, M. Avoiding Fractional Electrons in Subsystem DFT Based Ab-Initio Molecular Dynamics Yields Accurate Models For Liquid Water and Solvated OH Radical. *J. Chem. Phys.* **2016**, *144*, 234105.

(20) Neugebauer, J.; Louwerse, M. J.; Baerends, E. J.; Wesolowski, T. A. The merits of the frozen-density embedding scheme to model solvatochromic shifts. *J. Chem. Phys.* **2005**, *122*, 094115.

(21) Neugebauer, J. Chromophore-Specific Theoretical Spectroscopy: From Subsystem Density Functional Theory to Mode-Specific Vibrational Spectroscopy. *Phys. Rep.* **2010**, *489*, 1−87.

(22) Jacob, C. R.; Visscher, L. Calculation of Nuclear Magnetic Resonance Shieldings Using Frozen-Density Embedding. *J. Chem. Phys.* **2006**, *125*, 194104.

(23) Bulo, R. E.; Jacob, C. R.; Visscher, L. NMR Solvent Shifts of Acetonitrile from Frozen Density Embedding Calculations. *J. Phys. Chem. A* **2008**, *112*, 2640−2647.

DOI: 10.1021/acs.jpclett.9b03281
J. Phys. Chem. Lett. 2020, 11, 272−279

(24) Neugebauer, J.; Louwerse, M. J.; Belanzoni, P.; Wesolowski, T. A.; Baerends, E. J. Modeling Solvent Effects on Electron Spin Resonance Hyperfine Couplings by Frozen-Density Embedding. *J. Chem. Phys.* **2005**, *123*, 114101.
(25) Kevorkyants, R.; Wang, X.; Close, D. M.; Pavanello, M. Calculating Hyperfine Couplings in Large Ionic Crystals Containing Hundreds of QM Atoms: Subsystem DFT is the Key. *J. Phys. Chem. B* **2013**, *117*, 13967−13974.
(26) Wesolowski, T. A. Application of the DFT-based embedding scheme using an explicit functional of the kinetic energy to determine the spin density of Mg^{+} embedded in Ne and Ar matrices. *Chem. Phys. Lett.* **1999**, *311*, 87−92.
(27) Neugebauer, J.; Curutchet, C.; Munioz-Losa, A.; Mennucci, B. A Subsystem TDDFT Approach for Solvent Screening Effects on Excitation Energy Transfer Couplings. *J. Chem. Theory Comput.* **2010**, *6*, 1843−1851.
(28) Casida, M. E.; Wesolowski, T. A. Generalization of the Kohn−Sham Equations with Constrained Electron Density Formalism and Its Time-Dependent Response Theory Formulation. *Int. J. Quantum Chem.* **2004**, *96*, 577−588.
(29) Pavanello, M. On the Subsystem Formulation of Linear-Response Time-Dependent DFT. *J. Chem. Phys.* **2013**, *138*, 204118.
(30) García-Lastra, J. M.; Wesolowski, T. A.; Barriuso, M. T.; Aramburu, J. A.; Moreno, M. Optical and vibrational properties of MnF_6^{4-} complexes in cubic fluoroperovskites: insight through embedding calculations using Kohn-Sham equations with constrained electron density. *J. Phys.: Condens. Matter* **2006**, *18*, 1519−1534.
(31) Ramos, P.; Pavanello, M. Constrained Subsystem Density-Functional Theory. *Phys. Chem. Chem. Phys.* **2016**, *18*, 21172.
(32) Umerbekova, A.; Zhang, S.-F.; Kumar, S. P.; Pavanello, M. Dissecting energy level renormalization and polarizability enhancement of molecules at surfaces with subsystem TDDFT. *Eur. Phys. J. B* **2018**, *91*, 214.
(33) Pavanello, M.; Van Voorhis, T.; Visscher, L.; Neugebauer, J. An Accurate and Linear-Scaling Method for Calculating Charge-Transfer Excitation Energies and Diabatic Couplings. *J. Chem. Phys.* **2013**, *138*, 054101.
(34) Solovyeva, A.; Pavanello, M.; Neugebauer, J. Describing long-range charge-separation processes with subsystem density-functional theory. *J. Chem. Phys.* **2014**, *140*, 164103.
(35) Ramos, P.; Pavanello, M. Performance of Frozen Density Embedding for Modeling Hole Transfer Reactions. *J. Phys. Chem. B* **2015**, *119*, 7541−7557.
(36) Tölle, J.; Gomes, A. S. P.; Ramos, P.; Pavanello, M. Charged-cell periodic DFT simulations via an impurity model based on density embedding: Application to the ionization potential of liquid water. *Int. J. Quantum Chem.* **2019**, *119*, No. e25801.
(37) Götz, A.; Beyhan, S.; Visscher, L. Performance of Kinetic Energy Functionals for Interaction Energies in a Subsystem Formulation of Density Functional Theory. *J. Chem. Theory Comput.* **2009**, *5*, 3161−3174.
(38) Wesolowski, T. A.; Chermette, H.; Weber, J. Accuracy of approximate kinetic energy functionals in the model of Kohn-Sham equations with constrained electron density: The FH···NCH complex as a test case. *J. Chem. Phys.* **1996**, *105*, 9182.
(39) Laricchia, S.; Constantin, L. A.; Fabiano, E.; Sala, F. D. Laplacian-Level Kinetic Energy Approximations Based on the Fourth-Order Gradient Expansion: Global Assessment and Application to the Subsystem Formulation of Density Functional Theory. *J. Chem. Theory Comput.* **2014**, *10*, 164−179.
(40) Sinha, D.; Pavanello, M. Exact Kinetic Energy Enables Accurate Evaluation of Weak Interactions by the FDE-vdW Method. *J. Chem. Phys.* **2015**, *143*, 084120.
(41) Schlüns, D.; Klahr, K.; Mück-Lichtenfeld, C.; Visscher, L.; Neugebauer, J. Subsystem-DFT potential-energy curves for weakly interacting systems. *Phys. Chem. Chem. Phys.* **2015**, *17*, 14323−14341.
(42) Chacón, E.; Alvarellos, J. E.; Tarazona, P. Nonlocal kinetic energy functional for nonhomogeneous electron systems. *Phys. Rev. B: Condens. Matter Mater. Phys.* **1985**, *32*, 7868−7877.
(43) Jiang, K.; Nafziger, J.; Wasserman, A. Constructing a non-additive non-interacting kinetic energy functional approximation for covalent bonds from exact conditions. *J. Chem. Phys.* **2018**, *149*, 164112.
(44) Wesolowski, T. A.; Wang, Y. A. *Recent progress in orbital-free density functional theory*; World Scientific, 2013; Vol. 6.
(45) Karasiev, V. V.; Trickey, S. B. Issues and challenges in orbital-free density functional calculations. *Comput. Phys. Commun.* **2012**, *183*, 2519−2527.
(46) Witt, W. C.; Beatriz, G.; Dieterich, J. M.; Carter, E. A. Orbital-free density functional theory for materials research. *J. Mater. Res.* **2018**, *33*, 777−795.
(47) Nafziger, J.; Wasserman, A. Fragment-based treatment of delocalization and static correlation errors in density-functional theory. *J. Chem. Phys.* **2015**, *143*, 234105.
(48) Pavanello, M.; Neugebauer, J. Modelling Charge Transfer Reactions with the Frozen Density Embedding Formalism. *J. Chem. Phys.* **2011**, *135*, 234103.
(49) Ramos, P.; Mankarious, M.; Pavanello, M. *Practical Aspects in Computational Chemistry IV*; Springer, 2016; Chapter 4.
(50) Fermi, E. Un Metodo Statistico per la Determinazione di alcune Prioprietà dell'Atomo. *Rend. Accad. Naz. Lincei* **1927**, *6*, 602−607.
(51) Thomas, L. A. The calculation of atomic fields. *Math. Proc. Cambridge Philos. Soc.* **1927**, *23*, 542−548.
(52) von Weizsäcker, C. F. Zur Theorie der Kernmassen. *Eur. Phys. J. A* **1935**, *96*, 431−458.
(53) Wang, Y. A.; Carter, E. A. In *Theoretical Methods in Condensed Phase Chemistry*; Schwartz, S. D., Ed.; Kluwer: Dordrecht, 2000; pp 117−184.
(54) Wang, Y. A.; Govind, N.; Carter, E. A. Orbital-free kinetic-energy functionals for the nearly free electron gas. *Phys. Rev. B: Condens. Matter Mater. Phys.* **1998**, *58*, 13465−13471.
(55) Wang, Y. A.; Govind, N.; Carter, E. A. Orbital-free kinetic-energy density functionals with a density-dependent kernel. *Phys. Rev. B: Condens. Matter Mater. Phys.* **1999**, *60*, 16350−16358.
(56) Huang, C.; Carter, E. A. Nonlocal orbital-free kinetic energy density functional for semiconductors. *Phys. Rev. B: Condens. Matter Mater. Phys.* **2010**, *81*, 045206.
(57) Wang, L.-W.; Teter, M. P. Kinetic-energy functional of the electron density. *Phys. Rev. B: Condens. Matter Mater. Phys.* **1992**, *45*, 13196−13220.
(58) Mi, W.; Genova, A.; Pavanello, M. Nonlocal kinetic energy functionals by functional integration. *J. Chem. Phys.* **2018**, *148*, 184107.
(59) Pearson, M.; Smargiassi, E.; Madden, P. A. Ab initio molecular dynamics with an orbital-free density functional. *J. Phys.: Condens. Matter* **1993**, *5*, 3221−3240.
(60) Smargiassi, E.; Madden, P. A. Orbital-free kinetic-energy functionals for first-principles molecular dynamics. *Phys. Rev. B: Condens. Matter Mater. Phys.* **1994**, *49*, 5220−5226.
(61) Perrot, F. Hydrogen-hydrogen interaction in an electron gas. *J. Phys.: Condens. Matter* **1994**, *6*, 431−446.
(62) Mi, W.; Pavanello, M. Orbital-Free DFT Correctly Models Quantum Dots When Asymptotics, Nonlocality and Nonhomogeneity Are Accounted For. *Phys. Rev. B: Condens. Matter Mater. Phys.* **2019**, *100*, 041105.
(63) Perdew, J. P.; Burke, K.; Ernzerhof, M. Generalized Gradient Approximation Made Simple. *Phys. Rev. Lett.* **1996**, *77*, 3865−3868.
(64) Grafova, L.; Pitonak, M.; Rezac, J.; Hobza, P. Comparative Study of Selected Wave Function and Density Functional Methods for Noncovalent Interaction Energy Calculations Using the Extended S22 Data Set. *J. Chem. Theory Comput.* **2010**, *6*, 2365−2376.
(65) Giannozzi, P.; Baroni, S.; Bonini, N.; Calandra, M.; Car, R.; Cavazzoni, C.; Ceresoli, D.; Chiarotti, G. L.; Cococcioni, M.; Dabo, I.; et al. QUANTUM ESPRESSO: a modular and open-source software project for quantum simulations of materials. *J. Phys.: Condens. Matter* **2009**, *21*, 395502.

DOI: 10.1021/acs.jpclett.9b03281
J. Phys. Chem. Lett. 2020, 11, 272−279

(66) Sabatini, R.; Gorni, T.; De Gironcoli, S. Nonlocal van der Waals density functional made simple and efficient. *Phys. Rev. B: Condens. Matter Mater. Phys.* **2013**, *87*, 041108.
(67) Vanderbilt, D. Soft self-consistent pseudopotentials in a generalized eigenvalue formalism. *Phys. Rev. B: Condens. Matter Mater. Phys.* **1990**, *41*, 7892−7895.
(68) Garrity, K. F.; Bennett, J. W.; Rabe, K. M.; Vanderbilt, D. Pseudopotentials for high-throughput DFT calculations. *Comput. Mater. Sci.* **2014**, *81*, 446−452.
(69) See Supporting Information for additional tables and figures.
(70) Raghavachari, K.; Trucks, G. W.; Pople, J. A.; Head-Gordon, M. A fifth-order perturbation comparison of electron correlation theories. *Chem. Phys. Lett.* **1989**, *157*, 479−483.
(71) Vydrov, O. A.; Van Voorhis, T. Benchmark Assessment of the Accuracy of Several van der Waals Density Functionals. *J. Chem. Theory Comput.* **2012**, *8*, 1929−1934.
(72) Medvedev, M. G.; Bushmarinov, I. S.; Sun, J.; Perdew, J. P.; Lyssenko, K. A. Density functional theory is straying from the path toward the exact functional. *Science* **2017**, *355*, 49−52.
(73) Wasserman, A.; Nafziger, J.; Jiang, K.; Kim, M.-C.; Sim, E.; Burke, K. The Importance of Being Inconsistent. *Annu. Rev. Phys. Chem.* **2017**, *68*, 555−581.

DOI: 10.1021/acs.jpclett.9b03281
J. Phys. Chem. Lett. 2020, 11, 272−279